XII National and III International

Conference on Engineering Thermodynamics

12CNIT-2022 - FULL PAPER

Extension of Locally Adapted Models of Photosynthetically Active Radiation for All Sky Conditions

Ana García Rodríguez[1], Sol García Rodríguez[1], Diego Granados López[1], Elena Garrachón Gómez[1], Montserrat Díez Mediavilla[1]

[1]Solar and Wind Feasibility Technologies Research Group (SWIFT), Electromechanical Engineering Department, University of Burgos, 09006 Burgos, Spain. E-mail: agrodriguez@ubu.es

Keywords: *Solar Radiation; Modelling; PAR; biomass*

TOPIC:Renewable energies, environmental impact and circularity

1. Introduction

Photosynthetically Active Radiation (PAR, 400-700 nm) is the energy source to trigger photosynthesis. This process makes food and biomass production [1] and forest productivity possible [2], so it becomes essential for determining the impact of deforestation and climate change on agriculture [3]. Due to the scarcity of PAR data from direct measurements at ground meteorological stations, empirical models based on linear regressions have been developed for estimate PAR data [4], using other meteorological and climatic variables. In recent years, machine learning algorithms have been discovered as a useful tool for modelling meteorological and climatic data. Thus, Artificial Neural Networks (ANN) have been used for modelling PAR, with different meteorological variables as input [5]. Both procedures, multilinear regressions and ANN's, have been used in this work for modelling PAR in Burgos (Spain) under all sky conditions attending to the sky clearness classification and in an hourly basis. The performance of the resulting models has been tested for PAR estimates at other locations. To this end, he experimental data obtained from the Surface Radiation Budget Network (SURFRAD) in the USA was used. This proves the good fit of the models developed in Burgos to the SURFRAD weather stations.

2. Materials and method

The meteorological ground-station located at the Higher Polytechnic School (EPS) of the University of Burgos and described in detail in previous works [6] provided the meteorological and radiative data necessary for the study. The following variables were measured: air temperature and pressure (T, P), horizontal global irradiance ($RaGH$) and PAR. Data were recorded every 10 minutes and filtered according to conventional quality criteria [7]. Other necessary variables were derived from meteorological measurements, *i.e.*, cosine of the solar azimuth ($cosZ$), clearness index (k_t), horizontal diffuse fraction (k_d), and sky's clearness (ε) and brightness (Δ).

The experimental campaign took place from April 2019 to February 2021. Experimental data recorded at seven weather stations belonging to the SURFRAD network were also used. Figure 2 shows the location of the weather station in Burgos and the location of the seven SURFRAD weather stations. The measurement campaign covered from January 2009 to December 2018 at each station, with a temporal resolution of 1 min. Ten-minute values were obtained by averaging the original ones.

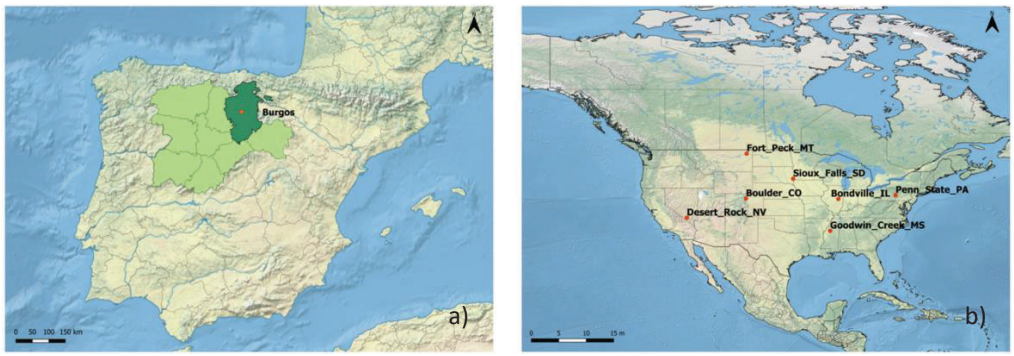

Figure 1. Location of the Burgos meteorological station (a) and the seven SURFRAD stations (b).

Each meteorological index (MI) described in Table 1 was determined both at the Burgos station and at each of the SURFRAD network stations. As explained above, T, P, $RaGH$, and PAR were obtained directly from experimental measurements. PAR was obtained from Q_p data ($\mu mol \cdot m^{-2} \cdot s^{-1}$) and transformed into power units ($W \cdot m^{-2}$) from the McCree's conversion factor ($\mu mol \cdot J^{-1}$) [8] . All other meteorological indices were calculated.

Table 1. Meteorological indices (MI's) measured and calculated in Burgos.

MI	MI	Expression	Ref.
$RaGH$	global horizontal irradiance	measured	-
k_d	diffuse fraction	$k_d = \frac{RaDH}{RaGH}$	[9]
Q_p	photosynthetically photon flux density	measured	-
PAR	photosynthetically active radiation	$PAR = \frac{Q_p}{4.57\mu mol} \cdot J^{-1}$	[8]
k_t	clearness index	$k_t = \frac{RaGH}{B_{sc} \cdot \varepsilon_0 \cdot cosZ_s}$	[10]
T	air temperature	measured	-
P	Air pressure	measured	-
T_d	dew point temperature	$T_d = \frac{35.859 \cdot logP_v - 21.48.496}{logP_v - 10.2858}$	[11]
$cosZ$	cosine of the solar azimuth	$cosZ = sin\delta \cdot sin\phi + cos\delta \cdot cos\phi \cdot cos\omega$	[10]
ε	sky's clearness	$\varepsilon = \frac{\frac{RaDH + RaB}{RaDH} + 1.04 \cdot Z_s^3}{1 + 1.04 \cdot Z_s^3}$	[12]
Δ	sky's brightness	$\Delta = \frac{m \cdot RaDH}{B_{sc} \cdot \varepsilon_0 \cdot cosZ_s}$	[12]

$\varepsilon_0 = 1 + 0.033 \cdot cos[2 \cdot \pi \cdot d_n/365]$ is the average value of the orbital eccentricity of the Earth. d_n is the day of the year. B_{sc} is the solar constant (1361.1 W/m^2 [13]).

Sky conditions were classified as clear, partial, and overcast using the clearness index (k_t) [14]. After that, a feature selection process was performed to select the most influent MI's on PAR data using Pearson coefficient [15] [8] for each sky type. Once the most influential variables, according to each sky category, those with a Pearson's coefficient greater than 0.5 were selected. PAR estimation models were developed for each of the three sky conditions (clear, partial and overcast skies), using both multilinear regressions (MLRs) and Artificial neural networks (ANNs) trained with the Levenberg-Marquardt Back-Propagation (LMBP) algorithm [16].

To study the goodness of fit of the models developed by means of MLRs and ANNs, the coefficient of determination (R^2), the normalized root mean square error ($nRMSE$) and the normalized mean bias error ($nMBE$) were used, Equations (1)-(3).

$$R^2 = \frac{\sum_{i=1}^{n}(PAR_{mod} - \overline{PAR_{mod}}) \cdot \left(PAR_{exp} - \overline{PAR_{exp}}\right)}{\sqrt{\sum_{i=1}^{n}(PAR_{mod} - \overline{PAR_{mod}})^2 \cdot \sum_{i=1}^{n}\left(PAR_{exp} - \overline{PAR_{exp}}\right)^2}}. \quad (1)$$

$$nRMSE\ (\%) = \frac{1}{\overline{PAR}_{exp}}\sqrt{\frac{\sum_{i=1}^{n}\left(PAR_{mod} - PAR_{exp}\right)^2}{n}} \cdot 100. \quad (2)$$

$$nMBE(\%) = \frac{1}{\overline{PAR}_{exp}}\frac{\sum_{i=1}^{n}\left(PAR_{mod} - PAR_{exp}\right)}{n} \cdot 100\,, \quad (3)$$

where n is the number of the experimental data used for fitting the models, PAR_{mod} are the modelled values of PAR, PAR_{exp} is the experimental value of PAR, $\overline{\mathrm{PAR}}_{\mathrm{exp}}$ is the mean of the experimental values and $\overline{\mathrm{PAR}}_{mod}$ is the mean of the calculated values.

3. Results and discussion

Based on the experimental data from Burgos, the most influential meteorological indices for each type of sky were found using Pearson's correlation coefficient. The results obtained are shown in Table 2.

Table 2. Pearson Coefficients, $r(PAR, MI_i)$, based on sky conditions defined by k_t sky classification (clear, partial, and overcast).

	$\lvert r(PAR, MI_i)\rvert$				
k_t interval	**[1-0.9]**	**(0.9-0.7]**	**(0.7-0.5]**	**(0.5-0.3]**	**(0.3,0]**
Clear	$RaGH, cosZ$		k_t, ε	T	k_d, Δ, P, T_d
Partial	$RaGH, cosZ$			T	$k_t, k_d, \Delta, \varepsilon, P, T_d$
Overcast	$RaGH$	$cosZ$	k_t, Δ		$k_d, \varepsilon, P, T, T_d$

From the results shown in Table 2, it can be observed that $RaGH$ is the meteorological index that has a very strong relationship with PAR for 3 skies types, coinciding with the results obtained by Ferrera-Cobos et al. [17]. Moreover, $cosZ$ also have a very strong or strong relationship with PAR, for the three sky conditions.

The models developed through multilinear regression taking into account the Pearson's coefficient presented in Table 2, are shown in Table 3.

Table 3. Multilinear regression models of PAR.

Sky type	Multilinear regression model	R^2	$nRSME$(%)
Clear	$PAR = -18.12 + 0.33RaGH + 83.15cosZ + 4.19 \cdot kt + 0.71\varepsilon$	0.990	3.27
Partial	$PAR = -1.81 + 0.40RaGH + 13.75cosZ$	0.977	6.80
Overcast	$PAR = -0.03 + 0.42RaGH + 6.88cosZ + 1.58k_t - 6.12\Delta$	0.978	7.33

By performing the PAR models using neural networks, very good fits have been obtained for the three sky types (Table 4). The best fit was obtained for clear skies, with a $R^2$of 0.992 and a $nRMSE$ of 3.01%.

Table 4. Statistical results of the ANN models.

Sky type	R^2	$nRMSE$ (%)	$nMBE$ (%)
Clear (ANN2)	0.992	3.01	$-4.68 \cdot 10^{-2}$
Partial (ANN3)	0.977	6.80	$4.06 \cdot 10^{-3}$
Overcast (ANN4)	0.978	7.28	$-3.50 \cdot 10^{-2}$

The models calibrated for Burgos were applied to the data measured at the seven stations of the SURFRAD network. Such stations are widely distributed throughout the USA. Statistical results showed that both methods, MLR models and ANN's, fitted well the SURFRAD experimental data, with R^2 higher than 0.98 and $nRMSE$ values lower than 10% for all locations and all sky conditions. The models for clear skies were the best fit at all weather stations, results are shown in Table 5.

Table 5. Model fit values for MLR (left) and ANN (right) models for clear sky conditions.

	MLR			ANN		
USA Stations	R^2	nRMSE (%)	nMBE (%)	R^2	nRMSE (%)	nMBE (%)
Bondville, Ilinois	0.985	4.05	1.61	0.985	4.13	1.28
Table Mountain, Boulder, Colorado	0.993	4.50	3.30	0.992	4.67	3.13
Desert Rock, Nevada	0.994	5.50	4.87	0.994	5.77	4.77
Fort Peck, Montana	0.988	5.41	4.16	0.987	5.31	3.74
Goodwin Creek, Missisippi	0.985	4.25	2.37	0.984	4.46	2.06

Penn State, Univ. Pennsylvania	0.987	3.77	1.20	0.986	4.02	0.95
Sioux Falls, South Dakota	0.991	5.44	4.49	0.990	5.36	4.03

4. Conclusions

The use of multilinear regressions and artificial neural networks is a very good technique to estimate PAR from different meteorological indices. The models obtained in Burgos for each sky type show very good fits. Moreover, these models are very well adapted to the seven locations in the USA, so it can be concluded that these models do not depend on the geographical location and that they are suitable for any sky condition.

Acknowledgments

Financial support was provided by the Spanish MCIN (Ref. RTI2018-098900-B-I00). Junta de Castilla y León provided financial support for Diego Granados López and Elena Garrachón Gómez (ORDEN EDU/556/2019 and Programa Operativo de Empleo Juvenil, Fondo Social Europeo, respectively).

References

[1] I. Alados, I. Foyo-Moreno, L. Alados-Arboledas, (1996) Photosynthetically active radiation: measurements and modelling. *Agricultural Forest Meteorology.* 78 pp 121–131.
[2] J.J. Landsberg, R.H. Waring, (1997) A generalised model of forest productivity using simplified concepts of radiation-use efficiency, carbon balance and partitioning. *Forest Ecology and Management*. 95 pp 209–228.
[3] P. Liu, X. Tong, J. Zhang, P. Meng, J. Li, J. Zhang, (2020) Estimation of half-hourly diffuse solar radiation over a mixed plantation in north China. *Renewable Energy*. 149 pp 1360–1369.
[4] S. Peng, Q. Du, A. Lin, B. Hu, K. Xiao, Y. Xi, (2015) Observation and estimation of photosynthetically active radiation in Lhasa (Tibetan Plateau). *Science Direct.* 55 pp 1604–1612.
[5] M. Roussenov, C. Huntingford, E.S. Jeffers, M.B. Bonsall, H.M. Christensen, T. Lees, (2019) Machine learning and artificial intelligence to aid climate change research and preparedness. *Enviorenmental Research.* 14.
[6] A. García-Rodríguez, D. Granados-López, S. García-Rodríguez, M. Díez-Mediavilla, C. Alonso-Tristán, (2021) Modelling Photosynthetic Active Radiation (PAR) through meteorological indices under all sky conditions. *Agricultural Forest Meteorology*. 310.
[7] C. Gueymard, J. Ruiz-Arias, (2016) Extensive worldwide validation and climate sensitivity analysis of direct irradiance predictions from 1-min global irradiance. *Solar Energy*. 128 pp 1–30.
[8] T. Akitsu, A. Kume, Y. Hirose, O. Ijima, K. Nasahara, (2015) On the stability of radiometric ratios of photosynthetically active radiation to global solar radiation in Tsukuba, Japan. *Agricultural Forest Meteorology.* 209–210 pp 59–68.
[9] D.G. Erbs, S.A. Klein, J.A. Duffle, (1982) Estimation of the diffuse radiation fraction for hourly, daily and monthly-average global radiation. *Solar Energy*. 28 pp 293–302.
[10] Iqbal M, (1983) An Introduction to solar radiation, Academic Press, New York, .
[11] R. and A.C.E. Society, American of Heating, (2015) Heating, Refrigeratingconditioning

Engineers American Society of Air-, in: ASHRAE Handb.
[12] R. Perez, P. Ineichen, R. Seals, J. Michalsky, R. Stewart, (1990) Modeling daylight availability and irradiance components from direct and global irradiance. *Solar Energy*. 44 pp 271–289.
[13] C.A. Gueymard, (2018) A reevaluation of the solar constant based on a 42-year total solar irradiance time series and a reconciliation of spaceborne observations. *Solar Energy*. 168 pp 2–9.
[14] A. Suárez-García, M. Díez-Mediavilla, D. Granados-López, D. González-Peña, C. Alonso-Tristán, (2020) Benchmarking of meteorological indices for sky cloudiness classification. *Solar Energy*. 195 pp 499–513.
[15] M.M. Mukaka, (2012) Statistics corner: A guide to appropriate use of correlation coefficient in medical research. *Malawi Medical. Journal.* 24 pp 69–71.
[16] Y.C. Du, A. Stephanus, (2018) Levenberg-marquardt neural network algorithm for degree of arteriovenous fistula stenosis classification using a dual optical photoplethysmography sensor. *Sensors.* 18.
[17] F. Ferrera-Cobos, J.M. Vindel, R.X. Valenzuela, J.A. González, (2020) Models for estimating daily photosynthetically active radiation in oceanic and mediterranean climates and their improvement by site adaptation techniques. *Advances in Space Research*. 65 pp 1894–1909.